Recovering 3D Structure of Nonuniform Refractive Space

Takahiro Higuchi, Fumihiko Sakaue and Jun Sato
Nagoya Institute of Technology, Japan
{*higuchi@cv., sakaue@, junsato@*}*nitech.ac.jp*

Keywords: Nonuniform Refractive Space, Refractive Index, 3D Structure, Ray Equation, Sparse Estimation.

Abstract: We present a novel method for recovering the whole 3D structure of a nonuniform refractive space. The refractive space may consist of a single nonuniform refractive medium such as heated air or multiple refractive media with uniform or nonuniform refractive indices. Unlike most existing methods for recovering transparent objects, our method does not have a limitation on the number of light refractions. Furthermore, our method can recover both gradual and abrupt changes in the refractive index in the space. For recovering the whole 3D structure of a nonuniform refractive space, we combine the ray equation in geometric optics with a sparse estimation of the 3D distribution. Testing showed that the proposed method can efficiently estimate the time varying 3D distribution of the refractive index of heated air.

1 INTRODUCTION

Various optical phenomena have been studied in the field of computer vision, and many advanced methods have been developed for recovering 3D structures from multiple views (Hartley and Zisserman, 2000; Faugeras and Luong, 2004; Agarwal et al., 2009), reflected light (Horn and Brooks, 1989; Woodham, 1980; Ikeuchi, 1981; Barron and Malik, 2015), refracted light (Murase, 1990; Kutulakos and Steger, 2005; Xue et al., 2014; Qian et al., 2016), and scattered light (Inoshita et al., 2012; Nishino et al., 2018). To make complex problems tractable, almost all methods are based on the assumption that light rays travel along straight lines or piecewise straight lines in 3D space.

However, if we look at light rays carefully, we find that they rarely go straight and that they almost always bend in 3D space, even in air, as shown in Fig. 1. Since the refractive index of air varies with the temperature (Owens, 1967), light rays refract everywhere in 3D space because of the nonuniform air temperature. They even bend around our body since the air temperature is not uniform around our body. In this paper, we consider such refraction of light rays at each point in the 3D space.

The refraction of light rays has long been studied for analyzing transparent objects, and many methods have been developed for recovering the 3D shape of transparent objects by observing the refraction of light rays (Murase, 1990; Kutulakos and Steger, 2005; Tian and Narasimhan, 2009; Xue et al., 2014; Qian et al., 2016). However, because of the complex nature of refraction, these methods suffer from several strong restrictions. Many of them are based on the assumption that the light refracts only once or twice (Murase, 1990; Tian and Narasimhan, 2009; Xue et al., 2014; Qian et al., 2016; Wetzstein et al., 2014), several are based on the assumption that the refractive index of the transparent object is known beforehand (Murase, 1990; Wetzstein et al., 2014), and almost all are based on the assumption that there is a distinct boundary for the refractive index, i.e. the object boundary, in the 3D space (Murase, 1990; Morris, 2007; Tian and Narasimhan, 2009; Wetzstein et al., 2014; Qian et al., 2016; Wu. et al., 2018). Hence, these methods cannot be used for recovering the 3D structure of a nonuniform refractive index distribution in 3D space.

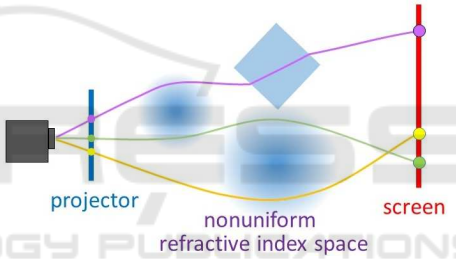

Figure 1: Recovery of 3D refractive index distribution of nonuniform refractive index space.

On the other hand, in the field of fluid dynamics, several methods have been developed for visualizing and recovering the 3D distribution of the refractive index in gas (Goldhahn and Seume, 2007; Atcheson et al., 2008; Ramanah et al., 2007; Stryczniewicz,

Higuchi, T., Sakaue, F. and Sato, J.
Recovering 3D Structure of Nonuniform Refractive Space.
DOI: 10.5220/0008940106540663
In *Proceedings of the 15th International Joint Conference on Computer Vision, Imaging and Computer Graphics Theory and Applications (VISIGRAPP 2020) - Volume 4: VISAPP*, pages 654-663
ISBN: 978-989-758-402-2; ISSN: 2184-4321
Copyright © 2022 by SCITEPRESS – Science and Technology Publications, Lda. All rights reserved

2018). However, these methods are specialized for gas flows, for which the change in refractive index is very small, and are based on the assumption that the light ray path can be approximated by a straight line in the refractive medium. Thus, if we consider the reconstruction of a larger variation in the refractive index in 3D space, such as the refractive index variation for solid and liquid objects, these methods are no longer applicable.

Therefore, in this paper, we describe the challenge of recovering an arbitrary refractive index distribution in 3D space and propose a method for recovering a fairly large variation in the refractive index distribution in a 3D space in which there are both gradual and abrupt changes in the refractive indices. For this objective, we project light rays from projectors and observe the points of light on a screen by using cameras, as shown in Fig. 1. The position of each point on the screen depends on the refractive index of every point on the corresponding light ray path. Hence, the position of a point on the screen includes information about the refractive index at all points along the path. Thus, we project a large number of light rays from a single or multiple projectors toward a nonuniform refractive index space and reconstruct the 3D refractive index distribution of the space from their points on the screen. However, if we have a large variation in the distribution, the reconstruction is very difficult. Thus, we propose an efficient two-step method that combines a linear model and a non-linear model of the light ray paths.

Since the boundary of the refractive index distribution is considered to be the boundary of a transparent object, the recovery of the 3D refractive index distribution can be considered the reconstruction of the whole 3D structure of a transparent scene.

2 RELATED WORK

Many methods have been reported for reconstructing transparent objects. However, since the light transport of typical transparent objects is very complicated, all of the existing methods have limited applicability.

Murase (Murase, 1990) pioneered a method for recovering the 3D shape of the surface of water in a tank from the image distortion of the texture on the bottom plane. Since then, the recovery of a water surface has been studied extensively. Tian and Narasimhan (Tian and Narasimhan, 2009) proposed a method for recovering the shape of the water surface and the texture of the bottom plane simultaneously. Morris and Kutulakos (Morris and Kutulakos, 2005) proposed a method for recovering an unknown refractive index and the surface shape of water using a known background pattern.

In the case of a water surface, the number of refractions is limited to one. However, solid transparent objects such as a glass accessory have more than one refraction, so recovering their surface shape is more difficult. Kutulakos and Steger (Kutulakos and Steger, 2005) investigated the feasibility of reconstruction under light ray refractions, and showed that three views are enough for recovering the light paths for up to two refractions. Qian et al. (Qian et al., 2016) used constraints on position and normal orientation at each surface point for recovering a 3D shape for up to two refractions. Kim et al. (Kim et al., 2017) proposed a method for recovering symmetric transparent objects when there are more than two refractions. For recovering nonsymmetric objects with more than two refractions, Wu et al. (Wu. et al., 2018) proposed a shape-recovery method based on both ray constraints and silhouette information. Using both space curving and ray tracing, their method can reconstruct complex nonsymmetric transparent objects from images.

Although these methods improve the shape recovery of solid transparent objects drastically, they are all based on the assumption that the light rays are piecewise linear and that they refract only at the surface of objects, more precisely at the boundary between media. The media type is unlimited, but each medium must be homogeneous and have a constant refractive index. This assumption is valid for most solid objects. However, if we consider more complex objects, such as heated air or a liquid mixture, these methods are no longer applicable. Xue et al. (Xue et al., 2014) proposed a method for recovering the nonuniform refractive index in gas. However, the gas is assumed to be a thin film, so the incoming light refracts only once in the gas.

For visualizing and recovering nonuniform refractive index distributions, such as that in a gas flow, the background oriented schlieren (BOS) method has been proposed in the field of fluid dynamics (Dalziel et al., 2000; Raffel et al., 2000). The BOS method first obtains the displacement vectors of a random dot pattern behind nonuniform refractive media and then uses these vectors as the integrals of refraction in the viewing direction for tomographic reconstruction of the refractive index distribution (Goldhahn and Seume, 2007; Raffel, 2015). Several variants of the BOS method have been proposed that improve the accuracy of gas flow estimation. Venkatakrishnan and Meier (Venkatakrishnan and Meier, 2004) improved the stability of the BOS method by assuming that the objective gas flow is axisymmetric. Atcheson et al. (Atcheson et al., 2008) proposed a linear method

for estimating the gradient field of the refractive index distribution. However, their method requires a complex post integration to recover the refractive index distribution from its gradient field, and this post integration is based on the assumption that the boundary of the objective gas flow is available. Although these assumptions may be valid in the field of gas flow estimation, they are obviously not valid for cases in which the refractive index distribution is not symmetric and does not have a distinct distribution boundary, such as heat haze on a road. Moreover, since these methods use tomographic reconstruction, light ray refraction is assumed to be very small, so the light path can be approximated by a straight line. This approximation is valid if the refractive media is gas, as is assumed in these methods. However, if we want to reconstruct refractive indices with larger variations, such as for nonuniform solid or liquid objects, straight ray approximation is no longer valid, and the BOS methods suffer from large errors in 3D reconstruction.

Therefore, we present in this paper a novel method for recovering nonuniform refractive index distributions that may include both gradual and abrupt changes in the refractive index. Unlike the existing methods in computer vision, our method does not need to limit the number of refractions, its application is not limited to uniform objects, and there is no need to know the refractive index of the media beforehand. Thus, it can be applied to the 3D reconstruction of non-uniform refractive media, such as heat haze. Also, our method does not depend on the assumption of symmetry in the refractive index distribution or the existence of a distribution boundary, unlike the BOS methods in the field of gas flow estimation.

3 PARAMETRIC REPRESENTATION OF NONUNIFORM REFRACTIVE MEDIA

For reconstructing the refractive indices of the whole 3D space efficiently, here we represent the refractive index distribution parametrically by using a Fourier series representation, i.e., Fourier basis functions and their coefficients. Use of Fourier basis functions and their coefficients enables the refractive index distribution to be represented sparsely by using a small number of non-zero parameters.

Suppose we have a 1D continuous signal $n(x)$ that spans from $x = 0$ to $x = X$. By considering it as a repetitive signal with a period of $[0, X]$, we can represent it by using a Fourier series up to the Nth order:

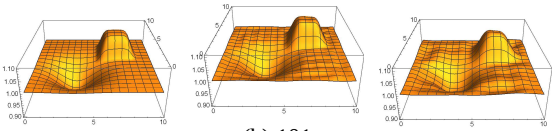

(a) original (b) 101 coefficients (c) 40 coefficients

Figure 2: Sparse Fourier series representation of refractive index distribution. Vertical axis shows refractive index at each point in 2D space. Both gradual and abrupt changes in refractive index distribution can be represented by using a small number of coefficients, as shown in (b) and (c).

$$n(x) = a_0 + \sum_{i=1}^{N} a_i \cos\frac{2i\pi x}{X} + b_i \sin\frac{2i\pi x}{X} \tag{1}$$

where a_0 and a_i, b_i $(i = 1, \cdots, N)$ are the Fourier coefficients, and these $2N+1$ coefficients represent the shape of the signal. In general, many coefficients in a_i and b_i are close to 0, so the signals can be represented by using a small number of coefficients.

By extending the 1D Fourier series representation, we can describe the refractive index distribution $n(x,y,z)$ in 3D space as

$$n(x,y,z) = \mathbf{Ba} \tag{2}$$

where $\mathbf{a} = [a_{000}, \cdots, a_{2N,2N,2N}]^\top$ represents a $(2N+1)^3$ vector consisting of the Nth order Fourier coefficients on the x, y, and z axes, and $\mathbf{B}$ represents a $(2N+1)^3$ vector consisting of 3D Fourier basis functions on the x, y, and z axes:

$$\mathbf{B} = \left[1, \cos\frac{2\pi x}{X}, \cdots, \sin\frac{2N\pi x}{X} \sin\frac{2N\pi y}{Y} \sin\frac{2N\pi z}{Z}\right] \tag{3}$$

where X, Y, and Z denote the size of the refractive index space along the x, y, and z axes, respectively. The reconstruction of the 3D refractive index distribution can then be considered as the estimation of the $(2N+1)^3$ Fourier coefficients, a_{ijk}, in $\mathbf{a}$.

For representing the abrupt changes in the refractive index distribution, we need high order terms in the Fourier coefficients vector $\mathbf{a}$, and hence we need to choose a large number as N. However, even in such cases, many coefficients in $\mathbf{a}$ are close to zero, so vector $\mathbf{a}$ is sparse. Thus, we estimate vector $\mathbf{a}$ by using a sparse estimation method in a later section.

Fig. 2 shows an example of a 2D refractive index distribution represented by Fourier coefficients in which both gradual and abrupt changes in the refractive index exist in the space. As shown in this figure, a small number of Fourier coefficients is enough for representing complex distributions.

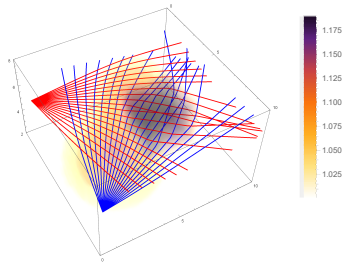

Figure 3: Ray tracing based on ray equation, Eq. (4). Light rays bend gradually or abruptly in accordance with gradient of refractive index field. Straight ray assumption used in BOS method is not valid under such strong refraction.

4 MODELING RAY REFRACTION

We next consider light ray refraction in nonuniform refractive index media.

If we have a glass object in air, there is a distinct boundary surface for the refractive index. In this case, the refraction of a light ray at the boundary surface can be described by Snell's law (Born and Wolf, 1980). However, if the refractive index changes continuously, such as for air with a nonuniform temperature, Snell's law is no longer applicable. In this case, the orientation of each light ray changes continuously in accordance with the refractive index distribution, so the change in orientation can be described by using the ray equation.

Suppose we have a nonuniform refractive index space. Let $n(\mathbf{x})$ be its refractive index at point $\mathbf{x} = [x,y,z]^\top$. Then, a light ray passing through $\mathbf{x}$ can be described by the following ray equation (Born and Wolf, 1980):

$$\frac{d}{ds}\left(n(\mathbf{x}(s))\frac{d\mathbf{x}(s)}{ds}\right) = \nabla\mathbf{n}(\mathbf{x}(s)) \qquad (4)$$

where s represents the position on the light ray, and $\nabla\mathbf{n}(\mathbf{x})$ denotes the gradient of n at point $\mathbf{x}$.

Since Eq. (4) is a 2nd order differential equation, a light ray path can be obtained by solving the differential equation using incident position $\mathbf{x}(0)$ and orientation $\frac{d\mathbf{x}(0)}{dt}$ of the light ray at $s = 0$. The solution of the differential equation can be obtained by using the Runge-Kutta method. Then, the position of the light ray at the screen can be derived by ray tracing using Eq. (4).

Fig. 3 shows an example of light rays in a nonuniform refractive index space that were derived from Eq. (4). The orientation of each light ray changes gradually or abruptly in accordance with the changes in the refractive index, so the straight ray assumption used in the BOS methods is not valid in this case.

5 RECONSTRUCTION OF REFRACTIVE INDEX DISTRIBUTION

We next describe our method for reconstructing 3D refractive index distributions from light ray positions on a screen. We calibrate the projectors, cameras, and the screen geometrically beforehand, so the light rays projected from the projectors and the screen points observed by the cameras are described in a single consistent set of 3D coordinates.

The fundamental strategy of our method is to find the coefficient vector $\mathbf{a}$ of the refractive index distribution that minimizes the error between light rays observed by the cameras and light rays synthesized from vector $\mathbf{a}$ by using the ray equation, Eq. (4). However, this minimization problem is easily trapped by local minima in general. Therefore, we propose an efficient two-step method for estimating coefficient vector $\mathbf{a}$. We describe each step below.

5.1 Linear Estimation of Initial Value

We first estimate Fourier coefficient vector $\mathbf{a}$ by using a linear approximation of the light ray model. This is similar to the method proposed by Atcheson et al. (Atcheson et al., 2008) but is different in a very important way. Atcheson et al. used a linear basis model to represent the gradient field, $\nabla\mathbf{n}(x,y,z)$, of the refractive index, $n(x,y,z)$, and estimated the coefficients of the model. After estimating the gradient field, they integrated the gradient field to estimate the refractive index distribution. However, this integration is noise sensitive, so it is not easy to obtain good results (Atcheson et al., 2008). Furthermore, it requires a distinct boundary for the gradient field, which is not always present in general cases. Thus, here we derive a method for estimating the refractive index distribution directly by using linear estimation. Since this approach does not require integration of the gradient field afterwards, computation is very stable and boundary information is not required.

Unlike Atcheson et al. (Atcheson et al., 2008), we use a linear basis model to represent the refractive index distribution directly, as shown in Eq. (2). Then, by taking its derivative, we can obtain the gradient field $\nabla\mathbf{n}(x,y,z)$ of the refractive index distribution $n(x,y,z)$:

$$\nabla\mathbf{n}(x,y,z) = \begin{bmatrix} \frac{\partial n(x,y,z)}{\partial x} \\ \frac{\partial n(x,y,z)}{\partial y} \\ \frac{\partial n(x,y,z)}{\partial z} \end{bmatrix} = \begin{bmatrix} \mathbf{B}_x \\ \mathbf{B}_y \\ \mathbf{B}_z \end{bmatrix} \mathbf{a} \qquad (5)$$

where $\mathbf{B}_x$, $\mathbf{B}_y$, and $\mathbf{B}_z$ denote the derivative of $\mathbf{B}$ with respect to x, y, and z, respectively.

Now, since the first term of $\mathbf{B}$ is equal to 1, the first terms of $\mathbf{B}_x$, $\mathbf{B}_y$, and $\mathbf{B}_z$ are equal to 0. Thus, Eq. (5) can be rewritten as:

$$\nabla \mathbf{n}(x,y,z) = \begin{bmatrix} \mathbf{B}'_x \\ \mathbf{B}'_y \\ \mathbf{B}'_z \end{bmatrix} \mathbf{a}' \tag{6}$$

where $\mathbf{a}'$, $\mathbf{B}'_x$, $\mathbf{B}'_y$, and $\mathbf{B}'_z$ are vectors made by dropping the first term in $\mathbf{a}$, $\mathbf{B}_x$, $\mathbf{B}_y$, and $\mathbf{B}_z$, respectively.

The important point here is that coefficients $\mathbf{a}$ in Eq. (2) are identical with coefficients $\mathbf{a}$ in Eq. (5), so they are identical with $\mathbf{a}'$ in Eq. (6) except the first term in vector $\mathbf{a}$. On the basis of this observation, we next propose a linear method for estimating coefficients $\mathbf{a}$ of refractive index distribution $n(x,y,z)$ directly by using its gradient field, $\nabla \mathbf{n}(x,y,z)$.

By taking the line integral of Eq. (4) along light ray path C in the nonuniform refractive index space, we have the relationship:

$$n(\mathbf{x})\frac{d\mathbf{x}}{ds} = \int_C \nabla \mathbf{n}(\mathbf{x})\, ds + \mathbf{d}_0 \tag{7}$$

where $\mathbf{d}_0$ is the input orientation of the light ray.

$\frac{d\mathbf{x}}{ds}$ in Eq.(7) represents the orientation of light ray $\mathbf{d}_1$ at the end of integral curve C, so it corresponds to the output orientation of the light ray. Assuming that the refractive index at the boundary of the observation area is 1.0 and substituting Eq. (6) into Eq. (7), we have the relationship:

$$\mathbf{d}_1 - \mathbf{d}_0 = \int_C \begin{bmatrix} \mathbf{B}'_x \\ \mathbf{B}'_y \\ \mathbf{B}'_z \end{bmatrix} \mathbf{a}'\, ds \tag{8}$$

Although the refractive index distribution is not uniform in the observation area, its coefficients $\mathbf{a}$ do not change in this area. Thus, Eq. (8) can be rewritten as:

$$\Delta \mathbf{d} = \mathbf{M}\mathbf{a}' \tag{9}$$

where $\Delta \mathbf{d} = \mathbf{d}_1 - \mathbf{d}_0$, and $\mathbf{M}$ is a $3 \times ((2N+1)^3 - 1)$ matrix derived by integrating the derivative of the basis functions:

$$\mathbf{M} = \int_C \begin{bmatrix} \mathbf{B}'_x \\ \mathbf{B}'_y \\ \mathbf{B}'_z \end{bmatrix} ds \tag{10}$$

Suppose we project L light rays from a single or multiple projectors. We then have:

$$\begin{bmatrix} \Delta \mathbf{d}_1 \\ \vdots \\ \Delta \mathbf{d}_L \end{bmatrix} = \begin{bmatrix} \mathbf{M}_1 \\ \vdots \\ \mathbf{M}_L \end{bmatrix} \mathbf{a}' \tag{11}$$

where $\Delta \mathbf{d}_i$ denotes $\Delta \mathbf{d}$ of the ith light ray, and $\mathbf{M}_i$ denotes matrix $\mathbf{M}$ computed from the ith light ray path C_i. Thus, if we know light ray path C_i $(i = 1, \cdots, L)$, matrix $\mathbf{M}_i$ $(i = 1, \cdots, L)$ can be computed, and coefficient vector $\mathbf{a}'$ can be estimated linearly from Eq. (11).

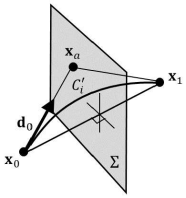

Figure 4: Integral curve C'_i defined by quadratic Bezier curve generated by three basis points, $\mathbf{x}_0$, $\mathbf{x}_1$, and $\mathbf{x}_a$ which is on symmetric plane Σ and in direction $\mathbf{d}_0$.

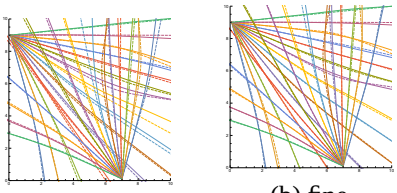

(a) sparse linear (b) fine estimation

Figure 5: Light rays obtained using sparse linear estimation and fine estimation. Solid lines and dashed lines show estimated rays and ground truth rays, respectively. Obtained rays converge to ground truth rays after fine estimation.

However, light ray path C_i in a nonuniform refractive index space is not known beforehand. Therefore, we approximate it by using a quadratic curve that passes through input point $\mathbf{x}_0$ and output point $\mathbf{x}_1$ in the observation area and has orientation $\mathbf{d}_0$ at the input point. Since there exists an infinite number of such quadratic curves, we choose a symmetric one with respect to the input and output points. Such a quadratic curve, C'_i, can be obtained as a quadratic Bezier curve whose three basis points are input point $\mathbf{x}_0$, output point $\mathbf{x}_1$, and intersection point $\mathbf{x}_a$ between an input light ray line and a symmetric plane perpendicular to a line segment $\mathbf{x}_0\mathbf{x}_1$, as shown in Fig. 4. Once quadratic curve C'_i is computed, matrix $\mathbf{M}_i$ $(i = 1, \cdots, L)$ can be obtained from Eq. (10). We can also compute output orientation $\mathbf{d}_1$ by taking the derivative of C' with respect to s. Then, Fourier coefficient $\mathbf{a}'$ of the refractive index distribution can be estimated linearly from Eq. (11).

However, this linear method does not work well since Fourier coefficient vector $\mathbf{a}'$ of a refractive index distribution is sparse in general, and the coefficients estimated from Eq. (11) fit not only the objective distribution but also image noises. If we estimate only low order terms of $\mathbf{a}'$, we can avoid this problem, but the abrupt changes in the distribution cannot be recovered. Therefore, we estimate coefficient vector $\mathbf{a}'$ by using a sparse estimation method under linear constraints without reducing the order of the

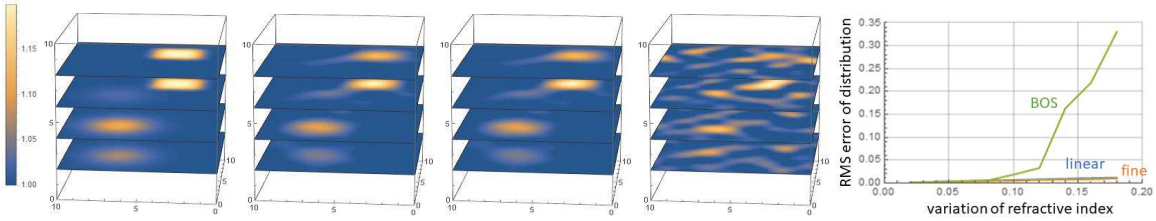

(a) ground truth (b) linear est. (c) fine est. (d) BOS method (e) RMSE

Figure 6: Cross-sectional views of refractive index distributions obtained using proposed method and existing BOS method in synthetic image experiments: (b) and (c) show distributions obtained using our sparse linear estimation and fine estimation, respectively. For comparison, (d) shows result using BOS method (Goldhahn and Seume, 2007). (e) shows relationship between magnitude of variation of refractive index distribution and RMS error of reconstructed distribution.

Fourier coefficients. We use Lasso (Tibshirani, 1996) and estimate sparse vector $\mathbf{a}'$ by solving the following minimization problem:

$$\hat{\mathbf{a}}' = \arg\min_{\mathbf{a}'} \sum_{i=1}^{L} \|\Delta\mathbf{d}_i - \mathbf{M}_i\mathbf{a}'\|^2 + \lambda\|\mathbf{a}'\|_1 \qquad (12)$$

where $\|\cdot\|_1$ denotes an L_1 norm, and λ denotes its weight. Once sparse Fourier coefficients $\mathbf{a}'$ are estimated, the refractive index distribution $n(x,y,z)$ can be obtained from Eq. (2). Since the first term a_{000} of the Fourier coefficients is indeterminate in this stage, we set $a_{000} = 1$ temporarily, and it is estimated in the following fine estimation stage.

The sparse linear method described in this section can estimate the refractive index distribution directly from the observed screen points, and it does not require post integration of the gradient field of the refractive index, unlike the method of Atcheson et al. (Atcheson et al., 2008). Thus, it is efficient and computationally stable.

5.2 Fine Estimation of Distribution

By using the sparse linear method described in section 5.1, we can roughly estimate refractive index distributions. However, the estimated distributions may have errors since the integral curve C' used in the linear model may deviate somewhat from the true light ray path. Thus, we next estimate the light ray path and the refractive index distribution simultaneously minimizing the observation error. The refractive index distribution estimated from the linear model is used as the initial value of this minimization.

Suppose we project L light rays from a single or multiple projectors toward a nonuniform refractive index space. Let $\mathbf{x}_i$ be the observed position of the ith light ray on the screen. We compute the light ray position, $\hat{\mathbf{x}}_i(\mathbf{a})$, on the screen by using ray tracing based on Eq. (4) in a refractive index distribution represented by Eq. (2). Then, we find the Fourier coefficients $\mathbf{a}$ that minimize $\sum_{i=1}^{L} \|\mathbf{x}_i - \hat{\mathbf{x}}_i(\mathbf{a})\|^2$.

In this estimation, we also want to fix the refractive index to 1.0 at the boundary of the observation area. This is achieved by minimizing cost function:

$$\mathbf{b}(\mathbf{a}) = \int_B \|1 - n(\mathbf{a})\|^2 ds \qquad (13)$$

where B denotes the boundary line of the observation area.

For estimating the sparse coefficients, we add the L_1 norm of vector $\mathbf{a}$ to the cost function. Thus, we estimate coefficients $\mathbf{a}$ of the refractive index distribution by solving the following minimization problem:

$$\hat{\mathbf{a}} = \arg\min_{\mathbf{a}} \sum_{i=1}^{L} \|\mathbf{x}_i - \hat{\mathbf{x}}_i(\mathbf{a})\|^2 + \mu\mathbf{b}(\mathbf{a}) + \lambda\|\mathbf{a}\|_1 \qquad (14)$$

where μ denotes the weight of the boundary error.

We used the steepest descent method to minimize the cost function and used coefficient vector $\mathbf{a}$ estimated using the method in section 5.1 as the initial value of this minimization problem. Once coefficients $\mathbf{a}$ are estimated from Eq. (14), the refractive index distribution $n(x,y,z)$ can be obtained from Eq. (2).

Fig. 5 shows the rays estimated using the sparse linear method described in section 5.1 and the fine estimation method described in section 5.2. The rays after fine estimation are almost identical to the ground truth rays, whereas those from sparse linear estimation deviate somewhat from the ground truth rays.

5.3 Recovery of Time Varying Distribution

We next extend our method for estimating time varying distributions. In most cases, the change in the distribution is continuous. Thus, we enhance the stability of the recovery by adding smoothness constraints in the time domain. Suppose we have a time series of observations, $\mathbf{x}_{ij}$ $(j = 1, \cdots, T)$. We estimate the

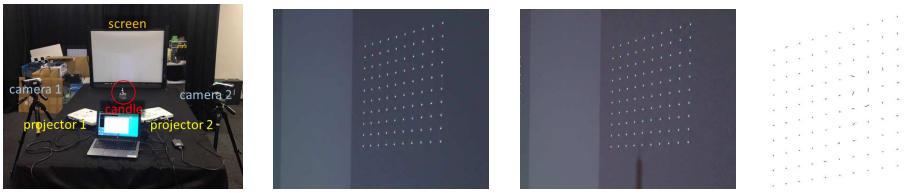

(a) experimental setup (b) without candle (c) with candle (d) deviation

Figure 7: Experimental setup and light rays projected on screen. (d) shows deviation in light rays caused by heated air.

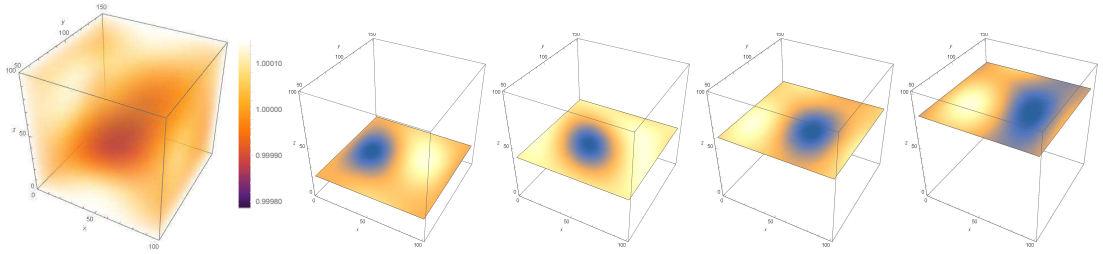

(a) refractive index distribution (b) $z = 20$ (c) $z = 40$ (d) $z = 60$ (e) $z = 80$

Figure 8: Refractive index distribution reconstructed with proposed method and cross-sectional views on four horizontal planes.

time series of coefficient vectors $\mathbf{a}_j$ $(j = 1, \cdots, T)$ as follows:

$$\{\hat{\mathbf{a}}_1, \cdots, \hat{\mathbf{a}}_T\} = \underset{\{\mathbf{a}_1, \cdots, \mathbf{a}_T\}}{\arg\min} \sum_{j=1}^{T} \sum_{i=1}^{L} \|\mathbf{x}_{ij} - \hat{\mathbf{x}}_i(\mathbf{a}_j)\|^2 + \mu \mathbf{b}(\mathbf{a}_j) + \lambda \|\mathbf{a}_j\|_1 + \kappa \mathcal{L}(\mathbf{a}_j) \quad (15)$$

where T denotes the number of time instants in the sequential observations, and $\mathcal{L}(\mathbf{a}_j)$ denotes a discrete Laplacian of $\mathbf{a}_j$ along the time axis. The smoothness is controlled by adjusting weight κ.

Once the time series of coefficients is obtained, the change in the refractive index distribution n_j can be recovered as follows:

$$n_j(x, y, z) = \mathbf{B}\mathbf{a}_j \quad (j = 1, \cdots, T) \quad (16)$$

In this way, we can recover a dynamic 3D refractive index space, such as heated air or mixture of different types of liquid.

6 EXPERIMENTS

6.1 Synthetic Image Experiment

To evaluate the performance of our proposed method, we first tested it by using synthetic images generated by projecting light rays into a synthetic nonuniform refractive index space. In this experiment, we used a nonuniform distribution that included both gradual and abrupt changes in the refractive index, as shown in Fig. 6 (a). The refractive index varied from 1.0 to 1.16. Since the variation of the refractive index of gas is $1.0 - 1.0005$, the variation in Fig. 6 (a) is quite large.

In our estimation, the refractive index distribution was modeled by a 6th order Fourier series, resulting in $13^3 = 2197$ parameters for coefficient vector $\mathbf{a}$. Using three projectors, we projected 108 rays of light in total. Then, 108 projected points on the screen were used for estimation.

Since each point on the screen provides three constraints on the distribution, we had $108 \times 3 = 324$ constraints in total. Although the number of parameters to be estimated exceeds the number of constraints obtained from the observation, our method can still recover the distribution since the coefficients are sparse and our method uses sparse estimation.

Fig. 6 (b) and (c) show the refractive index distributions estimated using our sparse linear estimation and fine estimation, respectively. The linear estimation derived a rough estimation of the distribution, and the fine estimation improved its accuracy. For comparison, the distribution obtained using the existing BOS method (Goldhahn and Seume, 2007) is shown in Fig. 6 (d). The BOS method could not recover the original distribution accurately, and there were many artifacts in the distribution. This is because the change in the refractive index was fairly large $(1.0 - 1.16)$, so the straight line assumption used in the BOS method was invalid.

Fig. 6 (e) shows the relationship between the mag-

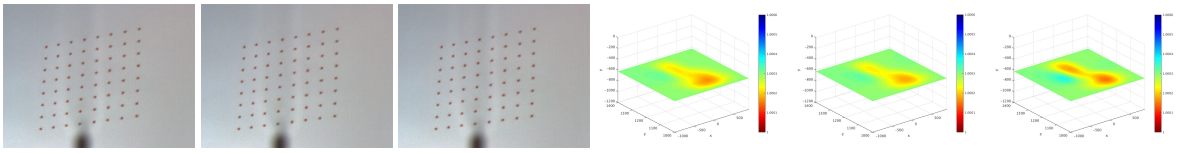

(a) time 1 (b) time 2 (c) time 3 (d) time 1 (e) time 2 (f) time 3

Figure 9: Three sequential images of rays on screen taken with camera at 30 fps, and cross-sectional view of reconstructed refractive index distribution at each time instant.

nitude of the variation of refractive index distribution and the RMS error of the reconstructed distribution. As we can see in this graph, the accuracy of the BOS method degrades rapidly under large variations of the refractive index while the proposed method is accurate even under large variations.

6.2 Real Image Experiment

We next evaluated the performance of our proposed method by using real images obtained from nonuniform refractive media. We positioned two projectors, two cameras, and a screen as shown in Fig. 7 (a) and reconstructed the nonuniform refractive media between the projectors and screen.

The thermal space around a candle flame was used as the nonuniform refractive index space. As mentioned above, the refractive index of air varies with the temperature. Thus, the 3D refractive index distribution of air heated by a candle flame is nonuniform. Moreover, since the temperature changes over time, the refractive index distribution of heated air also changes over time. We thus reconstructed the refractive index distribution at each time instant and recovered the dynamic change in the refractive index distribution.

We projected 64 rays from each projector toward the heated air and observed the resulting 128 points on the screen by capturing camera images at each time instant. Fig. 7 (b) and (c) show examples of points observed with and without the candle flame. The deviations in the light rays caused by the heated air are shown in Fig. 7 (d).

Again, since each point on the screen provides three constraints on the distribution, we had 384 constraints in total. We used 4th order Fourier coefficients to represent the distribution, so there was a total of 729 parameters for coefficient vector **a**. Again, the number of parameters exceeded the number of constraints obtained from the observation, but our method still recovered the distribution because of the sparse estimation.

Fig. 8 (a) shows the 3D refractive index distribution of heated air reconstructed using the proposed method from the images in Fig. 7. Fig. 8 (b) through (e) show cross-sectional views of the distribution for four horizontal planes. These results show that the nonuniform refractive index distribution of heated air can be recovered by using the proposed method.

We next recovered the refractive index distribution of a dynamically changing thermal space. Since the proposed method can recover the refractive index distribution from a single time image, it is possible to recover the temporal change in the refractive index, as described in section 5.3.

Fig. 9 shows three sequential images of rays on the screen captured with a camera at 30 fps and cross-sectional views of estimated changes in the refractive index distribution at three time instants. It shows that the refractive index distribution in a thermal space changes over time and that our method can recover these dynamic changes. These results demonstrate that, by using the proposed method, we can reconstruct the 3D structure of a dynamically changing transparent space.

6.3 Various Nonuniform Distributions

We next evaluated the performance of our method for various nonuniform refractive index distributions by using synthetic images. As shown in the first row of Fig. 10, we tested not only gradual changes in the refractive index but also abrupt changes, holes, and nested distributions. The second row in Fig. 10 shows the distributions estimated using our method, and the third row shows the results for the BOS method (Goldhahn and Seume, 2007). The table compares the accuracy of these two methods numerically. These results demonstrate that the proposed method outperforms the BOS method. In particular, the BOS method completely fails when the variation of distribution is large or abrupt, while the proposed method provides us good results even in such cases.

7 CONCLUSION

We have developed a method for recovering the whole refractive index distribution in a 3D space. The refractive index distribution is represented parametri-

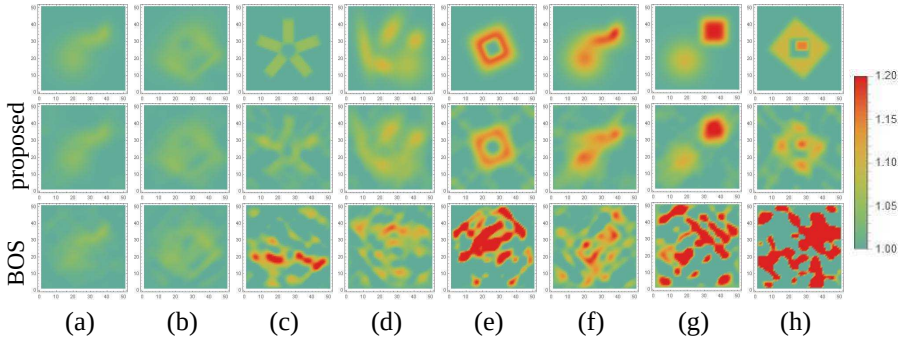

RMS Error		
	ours	BOS
(a)	0.0028	0.0038
(b)	0.0037	0.0051
(c)	0.0133	0.0730
(d)	0.0107	0.0426
(e)	0.0144	0.1516
(f)	0.0130	0.0546
(g)	0.0124	0.1677
(h)	0.0175	0.6445

Figure 10: Performance of proposed method for various nonuniform refractive index distributions. First row shows ground truth distributions, and second and third rows show distributions estimated using proposed method and BOS method (Goldhahn and Seume, 2007), respectively. Table shows corresponding RMS errors in recovered distributions. If variation of distribution is small, both methods provide us good results. However, if variation of distribution is large or abrupt, BOS method fails whereas our proposed method provides us good results.

cally and sparsely by using Fourier series representation. The complex refractive index distribution is reconstructed by combining a linear model and a nonlinear model of the light ray paths. The linear model is used to directly estimate the refractive index distribution simply by solving linear equations with sparseness constraints. The non-linear model is used to improve the accuracy of the distribution. Unlike existing methods, our method can recover the refractive index distribution of the whole 3D space, even if the space includes both gradual and abrupt changes in the refractive index. It can thus be used to recover the 3D structure of complex transparent scenes, such as heated air.

Evaluation of the proposed method using both synthetic and real images demonstrated its ability to reconstruct the refractive index distribution of a dynamically changing nonuniform refractive space.

Recovering the whole 3D structure of a transparent space is a very tough problem, and we have presented a method for efficiently solving this problem.

REFERENCES

Agarwal, S., Snavely, N., Simon, I., Sietz, S., and Szeliski, R. (2009). Building Rome in a day. In *Proc. IEEE International Conference on Computer Vision*.

Atcheson, B., Ihrke, I., Heidrich, W., Tevs, A., Bradley, D., Magnor, M., and Seidel, H.-P. (2008). Time-resolved 3D capture of non-stationary gas flows. *ACM Transactions on Graphics*, 27(5).

Barron, J. and Malik, J. (2015). Shape, illumination, and reflectance from shading. *IEEE Transaction on Pattern Analysis and Machine Intelligence*, 37(8):1670–1687.

Born, M. and Wolf, E. (1980). *Principles of optics: electromagnetic theory of propagation, interference and diffraction of light*. Elsevier.

Dalziel, S., Hughes, G., and Sutherland, B. (2000). Whole-field density measurements by 'synthetic schlieren'. *Experiments in Fluids*, 28(4):322–335.

Faugeras, O. and Luong, Q.-T. (2004). *The Geometry of Multiple Images*. MIT Press.

Goldhahn, E. and Seume, J. (2007). The background oriented schlieren technique: sensitivity, accuracy, resolution and application to a three-dimensional density field. *Experiments in Fluids*, 43(2–3):241–249.

Hartley, R. and Zisserman, A. (2000). *Multiple View Geometry in Computer Vision*. Cambridge University Press.

Horn, B. and Brooks, M. (1989). *Shape from Shading*. MIT Press.

Ikeuchi, K. (1981). Determining surface orientations of specular surfaces by using the photometric stereo method. *IEEE Transactions on Pattern Analysis and Machine Intelligence*, 3(6):661–669.

Inoshita, C., Mukaigawa, Y., Matsushita, Y., and Yagi, Y. (2012). Shape from single scattering for translucent objects. In *Proc. European Conference on Computer Vision*, pages 371–384.

Kim, J., Reshetouski, I., and Ghosh, A. (2017). Acquiring axially-symmetric transparent objects using single-view transmission imaging. In *Proc. IEEE Conference on Computer Vision and Pattern Recognition*, pages 1484–1492.

Kutulakos, K. and Steger, E. (2005). A theory of refractive and specular 3d shape by light-path triangulation. In *IEEE International Conference on Computer Vision*, volume 2, pages 1448–1455.

Morris, N. (2007). Reconstructing the surface of inhomogeneous transparent scenes by scatter-trace photography. In *IEEE International Conference on Computer Vision*.

Morris, N. and Kutulakos, K. (2005). Dynamic refraction stereo. In *IEEE International Conference on Computer Vision*, volume 2, pages 1573–1580.

Murase, H. (1990). Surface shape reconstruction of an undulating transparent object. In *Proc. IEEE International Conference on Computer Vision*, pages 313–317.

Nishino, K., Subpa-asa, A., Asano, Y., Shimano, M., and Sato, I. (2018). Variable ring light imaging: Capturing transient subsurface scattering with an ordinary camera. In *Proc. European Conference on Computer Vision*, pages 598–613.

Owens, J. (1967). Optical refractive index of air: dependence on pressure, temperature and composition. *Applied Optics*, 6(1).

Qian, Y., Gong, M., and Yang, Y. (2016). 3D reconstruction of transparent objects with position-normal consistency. In *Proc. IEEE Conference on Computer Vision and Pattern Recognition*, pages 4369–4377.

Raffel, M. (2015). Background-oriented schlieren (BOS) techniques. *Experiments in Fluids*, 56(3).

Raffel, M., Richard, H., and Meier, G. (2000). On the applicability of background oriented optical tomography for large scale aerodynamic investigations. *Experiments in Fluids*, 28(5):477–481.

Ramanah, D., Raghunath, S., Mee, D., Rosgen, T., and Jacobs, P. (2007). Background oriented schlieren for flow visualisation in hypersonic impulse facilities. *Shock Waves*, 17(1–2):65–70.

Stryczniewicz, W. (2018). Quantitative visualisation of compressible flows. *Transactions of the Institute of Aviation*, pages 132–141.

Tian, Y. and Narasimhan, S. (2009). Seeing through water: Image restoration using model-based tracking. In *Proc. IEEE International Conference on Computer Vision*, pages 2303–2310.

Tibshirani, R. (1996). Regression shrinkage and selection via the lasso. *Journal of the Royal Statistical Society. Series B*, 58(1):267–288.

Venkatakrishnan, L. and Meier, G. (2004). Density measurements using the background oriented schlieren technique. *Experiments in Fluids*, 37(2):237?–247.

Wetzstein, G., Heidrich, W., and Raskar, R. (2014). Computational schlieren photography with light field probes. *International Journal of Computer Vision*, 110(2):113–127.

Woodham, R. (1980). Photometric method for determining surface orientation from multiple images. *Optical Engineering*, 19(I):139–144.

Wu., B., Zhou, Y., Qian, Y., Cong, M., and Huang, H. (2018). Full 3d reconstruction of transparent objects. *ACM Transactions on Graphics*, 37(4).

Xue, T., Rubinstein, M., Wadhwa, N., Levin, A., Durand, F., and Freeman, W. (2014). Refraction wiggles for measuring fluid depth and velocity from video. In *Proc. European Conference on Computer Vision*.

SCITEPRESS SCIENCE AND TECHNOLOGY PUBLICATIONS